Published in final edited form as:
Biochemistry. 2008 December 9; 47(49): 12974–12984. doi:10.1021/bi800932c.

Probing the *Paracoccus denitrificans* cytochrome c_1 / c_{552} interaction by mutagenesis and fast kinetics†

Julia Janzon‡,*, **Quan Yuan**§, **Francesco Malatesta**‖, **Petra Hellwig**⊥, **Bernd Ludwig**‡,+, **Bill Durham**§, and **Francis Millett**§

‡*Molecular Genetics, Institute of Biochemistry, Biocentre Goethe-University, 60439 Frankfurt/Main, Germany*

§*Department of Chemistry and Biochemistry, University of Arkansas, Fayetteville, Arkansas 72701, US*

‖*Department of Pure and Applied Biology, University of L'Aquila, I-67010 L'Aquila, Italy*

⊥*Institut de Chimie - UMR 7177, Laboratoire de spectroscopie et électrochimie des biomolécules, Université Louis Pasteur 4, rue Blaise Pascal, 67070 Strasbourg, France*

+*Cluster of Excellence "Macromolecular Complexes" Goethe-University 60439 Frankfurt/Main, Germany*

Abstract

Electron transfer (ET) between *Paracoccus denitrificans* cytochrome c_1 and cytochrome c_{552} was studied using the soluble redox fragments cyt c_{1CF} and cyt c_{552F}. A new ruthenium cyt c_{552F} derivative labeled at C23 (Ru_z-23-c_{552F}) was designed to measure rapid electron transfer with cyt c_{1CF} in the physiological direction using flash photolysis. The bimolecular rate constant k_{12} decreased rapidly with ionic strength above 40 mM, consistent with a diffusional process guided by long-range electrostatic interactions between the two proteins. However, a new kinetic phase was detected below 35 mM ionic strength with the ruthenium photoexcitation technique in which k_{12} became very rapid (3×10^9 $M^{-1}s^{-1}$) and nearly independent of ionic strength, suggesting that the reaction became so fast that it was controlled by short-range diffusion along the protein surfaces guided by hydrophobic interactions. These results are consistent with a two-step model for formation of the final encounter complex. No intracomplex electron transfer between Ru_z-23-c_{552F} and c_{1CF} was observed even at the lowest ionic strength, indicating that the dissociation constant of the complex was greater than 30 μM. On the other hand, the ruthenium-labeled yeast cytochrome c derivative Ru_z-39-*Cc* formed a tight 1:1 complex with cyt c_{1CF} at ionic strengths below 60 mM with an intracomplex electron transfer rate constant of 50,000 s^{-1}. A group of cyt c_{1CF} variants in the presumed docking site were generated based on information from the yeast cyt bc_1/cyt *c* co-crystal structure. Kinetic analysis of cyt c_{1CF} mutants located near the heme crevice provided preliminary identification of the interaction site for cyt c_{552F}, and suggest that formation of the encounter complex is guided primarily by the overall electrostatic surface potential rather than by defined ions.

The mitochondrial respiratory chain consists of four redox protein complexes that transfer electrons from NADH (or $FADH_2$) to the terminal electron acceptor dioxygen. The free energy of these redox processes is used by three of the four transmembrane complexes to translocate protons across the inner mitochondrial membrane, thus generating an electrochemical proton gradient utilized by the ATP synthase to phosphorylate ADP (1). The cytochrome bc_1-complex

†This work was supported by Deutsche Forschungsgemeinschaft (SFB 472) and by NIH Grants GM20488 (FM and BD), and P20 RR15569.

*To whom correspondence should be addressed: Fax: (+49) 69-798-29515; Phone: (+49) 69-798-29127; Email: Janzon@nmr.uni-frankfurt.de .

represents the central core of the aerobic respiratory chain of eukaryotes and many prokaryotes. In bacteria, its simplest version consists of only the cofactor-containing subunits (2): the Rieske iron-sulfur protein (ISP), cytochrome *b* (cyt *b*) and cytochrome c_1 (cyt c_1)[1], whereas eukaryotes contain up to eight additional subunits, which may be involved in complex stability, assembly, or regulation (3–6).

The bc_1-complex of yeast mitochondria has been co-crystallized with its bound substrate, soluble cytochrome *c*, revealing insight into the cyt c_1 / cyt *c* interactions (7–9). A small, compact, mainly apolar binding site was identified, where direct contacts are mediated by hydrophobic interactions and a central cation-π interaction, with only two potential polar interactions. Similar results were obtained for several other cytochrome *c* redox complexes from different organisms using co-crystalization and X-ray approaches, as well as chemical shift perturbation mapping NMR experiments (8,10–13) and EPR measurements (14).

In contrast to this, mutagenesis and functional kinetic studies of the transient electron transfer (ET) reactions between cyt c_1 and cyt *c* revealed a clear electrostatic component. Acidic residues located around the heme cleft on cyt c_1 as well as lysine residues surrounding the heme crevice on cyt c were found to contribute to the Coulombic interaction (15–19). These results led to a two-step model for transient ET reactions describing the association of the two redox partners. Driven by long-range electrostatic interactions the redox partners approach each other, resulting in the formation of an encounter complex, which represents an ensemble of different relative orientations of both redox partners. Diffusion along the protein surfaces subsequently leads to the fine adjustment of both redox partners mediated by short-range hydrophobic interactions to yield the efficient complex, allowing fast ET (20–25).

The soil bacterium *P. denitrificans* expresses aerobic respiratory chain complexes which are homologous to its mitochondrial counterparts, yet are much simpler in subunit composition, thus making *P. denitrificans* a suitable model system for mitochondrial ET processes. The *Paracoccus* bc_1-complex consists of just three redox-active subunits (26). Cytochrome c_1 shows a tripartite domain structure (27): an N-terminal, highly acidic domain unique to *Paracoccus* is proposed, due to its strongly negative charge, to mimic the acidic hinge protein in bovine bc_1-complex (28) or subunit QCR6 in the yeast complex (6); the central core domain carries the covalently attached *c*-type heme group, and is followed by the C-terminal sequence for the membrane anchor. Electrons are passed from cyt c_1 to membrane bound cytochrome c_{552} (cyt c_{552}), which has been shown to be the genuine electron acceptor of the bc_1-complex (29). An electrostatic contribution to the interactions between cytochrome c_{552} and cyt c_1 has been deduced from kinetic investigations using genetically engineered soluble modules of both redox partners. The soluble cytochrome c_1 core fragment (cyt c_{1CF}) (27) consists of only the central core domain, lacking the acidic domain as well as the membrane anchor. The soluble

[1]**Abbreviations**

c_{1CF} : soluble cytochrome c_1 core fragment of *Paracoccus denitrificans*
c_{552F} : soluble cytochrome c_{552} fragment of *Paracoccus denitrificans*
cyt: cytochrome
DSC: double sector cuvette
ET: electron transfer
ISD: ionic strength dependency
FP: flash photolysis
P. d.: Paracoccus denitrificans
Ru_Z : Ru(2,2'-bipyrazine)$_2$(4-bromomethyl-4'-methyl-2,2'-bipyridine)
Ru_Z-23-c_{552F}: *Paracoccus denitrificans* cytochrome c_{552F} with surface asparagine 23 mutated to cysteine (N23C) and covalently attached to Ru_Z
Ru_Z-39-*Cc*: yeast iso-cytochrome *c* with cysteine 102 mutated to threonine (C102T) and introduced surface cysteine in position 39 (H39C), covalently attached to Ru_Z
SF : stopped-flow
WT: wild-type

cytochrome c_{552} fragment (cyt c_{552F}) (30) contains only the C-terminal hydrophilic heme carrying domain without the N-terminal membrane anchor and linker region. Both fragments can be regarded as minimal redox units of the native cytochromes, providing the advantage of simplified experimental design as no detergents are necessary to keep the cytochromes soluble. Moreover, the ET reaction of interest is not influenced by subsequent ET events or energy transduction steps, as in the case of redox complexes.

The transient nature of ET reactions between redox proteins has been previously studied using stopped-flow techniques (21,22,24,27,31–33) and EPR (14). In particular, the pre-steady state kinetics of terminal ET processes in the aerobic respiratory chains of *P. denitrificans* and *T. thermophilus* have been investigated using soluble fragments of membrane-bound redox proteins and soluble cytochromes c (21,22,24,31–33).

A ruthenium flash photolysis method has been developed to characterize both intracomplex and bimolecular ET between redox partners with microsecond time resolution, as well as ET within redox protein complexes such as the cyt bc_1 complex (32–39). A photo-excitable ruthenium complex is either covalently attached to one redox partner, or bound by electrostatic interactions (3,34–36). Photoexcitation of Ru(II) to Ru(II*) rapidly reduces or oxidizes the neighboring heme group, and induces subsequent ET events. The development and synthesis of ruthenium complexes with differing redox properties allowed the determination of ET processes in a number of redox systems (3), including intracomplex ET within the bc_1-complex of different organisms (3,34–36) and the intermolecular reaction between cyt *c* and cyt c_1 of the bc_1-complex (3,36).

Here we present the functional and dynamic characterization of the ET reaction between *P. denitrificans* cyt c_{1CF} and cyt c_{552F} using both stopped-flow spectroscopy and ruthenium photoexcitation techniques. To study the ET reaction between cyt c_{1CF} and cyt c_{552F} in the physiological direction, Ru_z-23-c_{552F} was prepared by covalently attaching the photo-excitable ruthenium compound Ru(2,2'-bipyrazine)$_2$(4-bromomethyl-4'-methyl-2,2'-bipyridine) (Ru_z) (3) to the single cysteine introduced on the surface of cyt c_{552F}N23C. The second-order rate constant of the reaction of Ru_z-23-c_{552F} with cyt c_{1CF} is the same as that of unlabeled cyt c_{552F} at 200 mM ionic strength, indicating that the ruthenium label does not affect the reaction under these conditions. The high time resolution of the ruthenium method allowed extension of the kinetic studies to low ionic strengths, where evidence for a two-step mechanism was observed.

To determine the interaction interface on *P. denitrificans* cyt c_1 for cyt c_{552}, a series of cyt c_{1CF} variants in the presumed docking site were prepared. The yeast cyt bc_1/cyt *c* co-crystal structure (7–9) was used in combination with sequence alignment and structural modelling to identify residues in the putative binding site of *P. denitrificans* cyt c_{1CF}, since structures of neither *P. denitrificans* cyt c_1 nor the c_1/c_{552}-complex are available. The side chain residues were varied in bulk, polarity or charge, and the kinetics of the reactions of the cyt c_{1CF} mutants with cyt c_{552F}, Ru_z-23-c_{552F}, and yeast Ru_z-39-Cc were examined.

Experimental Procedures

Site-directed mutagenesis, heterologous expression and purification procedures

Site-directed mutagenesis was performed using the QuikChange (Stratagene) or Altered sites (Promega) mutagenesis kits. pET-22b(+) (Novagen) and pAlter-Ex1 (Stratagene) served as templates for the cyt c_{1CF} mutagenesis reaction, with the cyt c_{1CF} gene cloned via *Nco*I and *Hin*dIII into the multiple cloning sites (for details see (27)).

For introducing the surface cysteine (N23C) into cyt c_{552F}, pBR2 (30) was taken as template. The following primers were used (mutagenic triplet in bold): **E243K**: 5'-C TTG CAG GTC TAT A*CC* **AAG** GTC TGC TCG G*CC* TGC-3'; **V244Q**: 5'-CAG GTC TAT A*CC* GAG **CAG** TGC TCG G*CC* TGC CAC-3'; **V244Q_rev:**5'-GTG GCA GGC CGA GCA GGT **CTC** GGT ATA GAC CTG-3', **V244T:** 5'-CAG GTC TAT A*CC* GAG **AC*C*** TGC TGC G*CC* TGC CAC-3'; **V244T_rev:** 5'-GTG GCA GGC CGA GCA **GGT** CTC GGT ATA GAC CTG-3'; **A247N:** 5'-A*CC* GAG GTC TGC TCG **AAC** TGC CAC GGC CTG CGC-3'; **A247N_rev:** 5'-GCG CAG G*CC* GTG GCA **GTT** CGA GCA GAC CTC GGT-3'; **A314S:** 5'-GAC CTG TCG CTG ATG **TCA** AAG GCG CGC G*CC* GGG-3'; **A314S_rev:** 5'-*CC*C GGC GCG CGC CTT **TGA** CAT CAG CGA CAG GTC-3'; **K315E:** 5'-CTG TCG CTG ATG G*CC* **GAG** GCG CGC G*CC* GGG TTC-3'; **K315E_rev:** 5'-GAA *CC*C GGC GCG CGC **CTC** GGC CAT CAG CGA CAG-3'; **K315T:** 5'-CTG TCG CTG ATG G*CC* **ACG** GCG CGC G*CC* GGG TTC-3'; **K315T_rev:** 5'-GAA *CC*C GGC GCG CGC **CGT** GGC CAT CAG CGA CAG-3'; **G319A:** 5'-G*CC* AAG GCG CGC G*CC* **GCG** TTC CAT GGC *CC*C TAC-3'; **G319A_rev:** 5'-GTA GGG G*CC* ATG GAA **CGC** GGC GCG CGC CTT GGC-3'; **S378A:** 5'-ATG GCG GCG *CC*C CTC **G*CC*** GAC GAC CAG GTC A*CC*-3'; **S378A_rev:** 5'-GGT GAC CTG GTC GTC **GGC** GAG GGG CGC CGC CAT-3'; **Q381V:** 5'-*CC*C CTC AGC GAC GAC **GTG** GTC A*CC* TAT GAG GAT-3'; **Q381V_rev:** 5'-ATC CTC ATA GGT GAC **CAC** GTC GTC GCT GAG GGG-3'; **T383C:** 5'-AGC GAC GAC CAG GTC **TGC** TAT GAG GAT GGC A*CC*-3';. c_{552F}_**N23C:** 5'-AAG CTG GAC GGC **TGC** GAT GGC GTC GGC *CC*G-3'; **N23C_rev:** 5'-CGG G*CC* GAC G*CC* ATC **GCA** G*CC* GTC CAG GTT-3'.

Cytochrome c_{552F} was expressed and purified as described by Reincke *et al.* (30). Cytochrome c_{1CF} and mutants were expressed heterologously in *E. coli* BL21(DE3) using pET-22b(+) (both Novagen) as IPTG-inducible expression plasmid, which provides the *pel*B leader sequence for periplasm transport of the apoprotein. Cotransformation with the heme maturation plasmid pEC86 (37) achieved efficient cofactor incorporation into the cytochrome. Cells were incubated at 37 °C and harvested 3–4 hours after induction with 0.4 mM IPTG, yielding around 4 mg of cyt c_{1CF} per liter of culture medium. The periplasm was prepared (38) and the cytochromes purified via ion exchange chromatography (Q-Sepharose *fast flow* (Amersham Bioscience) with 50 mM Tris/Cl pH 8.0, 50 mM NaCl, 2 mM EDTA; NaCl gradient: 50–500 mM) and gel filtration (Sephacryl S-100 (Amersham Bioscience) with 50 mM Tris/Cl pH 8.0, 150 mM NaCl, 2 mM EDTA). Purification steps were followed by SDS-PAGE (39) and Western blot analysis. Correct heme incorporation was demonstrated by heme staining (40), charge transfer and absorption (Supplement 1) redox difference spectra. In addition the X-ray and NMR-structures of cyt c_{552F} in both redox states are known (30,41) For precise cytochrome concentrations during the stopped-flow and laser flash experiments, extinction coefficients of each cyt c_{1CF} mutant were determined by pyridine hemochrome spectra (42) (see Supplement 2). Additionally, the redox potentials of cyt c_{1CF} wild-type and mutants were determined by redox titrations *versus* the standard hydrogen electrode at pH 7.0 (SHE') (see Supplement 2).

Pre-steady state stopped-flow kinetics

To bypass the problem of spectral overlap, wavelengths had to be found at which the ET reactions between the cytochromes could be detected. This was achieved by recording difference spectra using double sector cuvettes (DSC) (for details see (27)). The peaks and troughs of the DSC-spectra in the Soret and α-region display those wavelengths of minimal spectral overlap and maximal signal amplitude (see Supplement 2). All kinetic experiments were carried out using a thermostatted Applied Photophysics stopped-flow apparatus (Leatherhead, UK) with a 1 cm observation chamber. Nitrogen flushed Tris/Cl buffer was used (20 mM Tris/Cl pH 8.0, 20 mM KCl, 1 mM EDTA) and the ionic strength varied by adding appropriate amounts of solid KCl. Cyt c_{1CF} was pre-reduced with 0.5 mM ascorbate for at least 10 minutes before the measurements in a reaction slow enough not to interfere with the ET

reaction of interest (27). ET kinetics were studied in the physiological forward direction from cyt c_{1CF} to cyt c_{552F} at 4.8 °C. At least three kinetic traces were averaged and fitted, taking into account the prevalent non-pseudo first order conditions (for details see (27)). Bimolecular rate constants were plotted according to the Brønsted equation (43) to determine the ionic strength dependence of the reaction rates. Data fitting was performed using the Origin 7.5 (OriginLab Corporation) software. The standard deviation of the fitted parameters was below 10 %.

Preparation of Ru_z-23-c_{552F}

Site-directed mutagenesis was used to introduce a single cysteine at residue N23 on the surface of cyt c_{552F} remote from the putative reaction site with cyt c_1 (Figure 1). The ruthenium reagent Ru(2,2'-bipyrazine)$_2$(4-bromomethyl-4'-methyl-2,2'-bipyridine) (Ru_z) is highly selective for labelling only cysteine residues under the conditions used (39). N23C cyt c_{552F} (1.4×10^{-7} mol) was treated with a 10-fold molar excess of dithiothreitol (DTT) to reduce the cysteine, and concentrated and exchanged to 0.7 mM in a volume of 200 µL 50 mM sodium borate buffer, pH 9.0, using a Centricon Ultracel YM-10 concentrator. A 2-fold molar excess of DTT was added to the anaerobic solution of the protein, followed by the addition of a 3-fold molar excess of Ru(2,2'-bipyrazine)$_2$(4-bromomethyl-4'-methyl-2,2'-bipyridine)) with stirring. Ruthenium labeling was continued for 12–14 hours in the dark under anaerobic conditions at room temperature. The reaction mixture was then exchanged in 5 mM sodium phosphate buffer, pH 7.0, to lower the ionic strength and applied to a 5 mm × 50 mm DE53 column equilibrated with 5 mM sodium phosphate, pH 7.0. Only unlabelled N23C cyt c_{552F} strongly bound to the column while most of the labeled protein was eluted with 5 mM phosphate buffer. Ru_z-23-c_{552F} was purified by HPLC on a 1.5 cm × 30 cm high-resolution DEAE-52 column which can separate Ru_z-23-c_{552F} from possible impurities. Before loading the sample on the HPLC column, DTT (or ascorbate) was added to keep Ru_z-23-c_{552F} reduced and bound to the anion exchange column. A single major peak eluted off the DEAE-52 column which had a UV/visible spectrum equal to the sum of one equivalent of Ru_z-23-c_{552F} and one equivalent of Ru_z. The purified Ru_z-23-c_{552F} was exchanged three times with 5mM sodium phosphate, pH 7.0 buffer, then concentrated and frozen at −80 °C. The overall yield of Ru_z-23-c_{552F} was about 30 %, and most of the remaining 70 % was unlabeled N23C cyt *c*552F.

Flash photolysis experiments

Transient absorbance measurements of ET between Ru_z-23-c_{552F} and cyt c_{1CF} were carried out using a phase R model DL 1400 flash lamp-pumped dye laser generating a 480 nm excitation light pulse of 0.5 µs duration and a detection system described by Heacock *et al.* (44). Solutions contained about 5 µM Ru_z-23-c_{552F} and 1–20 µM cyt c_{1CF} in 300 µl of 10 mM Tris/Cl buffer pH 8.0 in semimicro glass cuvettes. Addition of 0.1–1.1 mM sodium ascorbate and 2 µM N, N, N',N'-tetramethylphenylendiamine (TMPD) achieved reduction of the heme groups. The sacrificial oxidant paraquat in oxygen-saturated buffer was used to reoxidize Ru (I) to Ru(II). Ionic strength conditions were varied by the addition of the appropriate volume of a 2 M KCl stock solution. The ET reaction was monitored at 550 and 558 nm. The reaction between yeast Ru-39-*Cc* and cyt c_{1CF} was studied under the same conditions except that 5 mM sodium phosphate, pH 7.0 was used as the buffer. All absorbance transients were analyzed using the KINFIT kinetics program obtained from On-line Instrument System Inc.. Absorbance spectra were obtained with a Hewlett-Packard 8452A diode array spectrophotometer.

Results and Discussion

Our aim was to characterize the ET reaction between *Paracoccus denitrificans* cyt c_{1CF} and cyt c_{552F} and identify those residues on cyt c_1 which contribute to the reaction. Since no structural data of *P. denitrificans* cytochrome c_1 or its complex with cytochrome c_{552} are

available, the yeast cyt bc_1/cyt *c* co-complex structure (6–9) was used as a guide for identifying putative residues at the binding domain. Although the yeast cyt bc_1-complex shows a bell-shaped ionic strength dependence of activity (45), the cyt cb_1/cyt c co-complex structure revealed a small compact contact site between cyt c_1 and cyt *c* with direct interactions mediated primarily by apolar contacts and a central cation-π-interaction between phe 230 of cyt c_1 and arg 13 of cyt *c*. No salt bridges or hydrogen bonds were observed within this non-polar contact area (9), but it is surrounded by a semicircle of oppositely charged ion-pairs, which are not in close contact, thus mediating weak electrostatic interactions (9).. We identified corresponding residues on *P. denitrificans* cyt c_1 by sequence alignment and structural modelling approaches, and varied the bulk, charge, or polarity of these residues by site-directed mutagenesis. The biochemical, spectral, and redox properties of the mutant proteins were fully characterized. In order to identify the interaction domain, the kinetics of the reaction between the cyt c_{1CF} mutants and cyt c_{552F} was studied using both the high speed ruthenium flash-photolysis method and stopped-flow spectroscopy.

Generation of the cyt c_{1CF} mutants and redox-biochemical characterization

Identification of the corresponding residues in *P. denitrificans* cyt c_1 was achieved by performing a sequence alignment (ClustalW, (46)), using the cyt c_1 sequences of *Rhodobacter capsulatus* (*Rc*), *Rhodobacter sphaeroides* (*Rs*), *Paracoccus denitrificans* (*Pd*), *Saccharomyces cerevisiae* (*Sc*) and *Bos taurus* (*Bt*)) (see Supplement 3). The alignment revealed a couple of gaps and sequence insertions between the pro- and eukaryotic sequences, as well as between the *P. denitrificans* and the *Rhodobacter* sequences, rendering the search for the corresponding cyt c_1 residues challenging. In case an aligned position was ambiguous, additional alternative mutagenesis positions were chosen. Cyt c_1 positions mediating direct interactions to cyt *c* within the yeast co-crystal, the corresponding residues in the *P. denitrificans* cyt c_1, and site-directed mutations are listed in Table 1.

In addition, the *P. denitrificans* cyt c_1 sequence was modelled onto the yeast cytochrome c_1 structure (1KYO, pdb (8)) using different approaches (Swissmodell (47), Jigsaw3D (48), Esypred (49)) to determine if the chosen amino acids of *Paracoccus* cyt c_1 are located at similar positions in the putative structure and show a similar orientation towards the potential interaction interface as in the yeast co-complex (see Figure 2 for the c_{1CF} Swissmodel structure). The overall modelled cyt c_{1CF} backbone fold was nearly identical to that of the 1KYO pdb-structure, displaying deviations only in the loop regions in agreement to the gaps and insertions in the sequence alignment. Mutated side chain positions showed a similar location and orientation within the different structural models as well as the yeast c_1-structure. The heme cleft is surrounded by surface-exposed acidic residues in a circular arrangement, which may be responsible for long-range electrostatic steering of both redox partners to form an encounter complex (see Figure 1 for the complementary heme hemisphere of cyt c_{552F}).

Based on the sequence alignment and structural models the mutated positions were grouped into three regions (region I–III, see Figure 2). Region I contains the mutations E243K, V244Q, V244T and A247N, which are all located within or directly preceding the heme binding motif cxxch in the amino acid sequence. This region is positioned directly above the heme crevice when viewed onto the membrane plane along the transmembrane helix (TMH) present in native cytochrome c_1. The position of the α-helical region II is ambiguous, as obtained by the different structural models, and contains the mutations A314S, K315E/T and G319A, all positions highly conserved in prokaryotes. Its most likely localization is below the heme crevice. Region III is located on the left in vicinity to region I and seems to be conserved in all structural models. As indicated by the sequence alignment, S378 within region III is the residue corresponding to F230 of yeast, which is seen in that structure (8) to mediate the cation-π-interaction. Residue Q381 corresponds to M233. Variants were generated by site-directed mutagenesis, expressed

heterologously in *E. coli*, purified, and biochemically characterized by SDS-PAGE, Western blot analysis and heme staining, confirming that all mutant proteins were identical to wild-type c_{1CF} (data not shown).

Stopped-flow kinetics of the ET reaction between cyt c_{1CF} wild-type and c_{552F}

The ET reaction between the cyt c_{1CF} WT and c_{552F} using pre-steady state stopped-flow techniques previously described (27), followed an optimized protocol dealing with the problems of spectral overlap, heme-autoxidation and non-pseudo-first order conditions. Using soluble modules of redox proteins of respiratory chain complexes as models for elucidation of electron transport mechanisms offers the advantage of simplified experimental procedures, as no detergent is required to keep the cytochromes in solution. Moreover, only the ET reaction of interest is followed and kinetic interference by subsequent internal ET or energy transduction steps is circumvented. However, it should be kept in mind that the reactions of soluble fragments in solution provide a higher degree of diffusional freedom compared to the reaction of membrane-anchored c_{552} with cyt c_1 in the transmembrane bc_1 complex, where the directionality of the ET interactions is physically much more restricted. By performing the kinetics at 8 °C, it was possible to resolve the bimolecular ET reaction down to an ionic strength of 70 mM. The second-order rate constant k_{12} was 2.3×10^8 $M^{-1}s^{-1}$ at 70 mM ionic strength, decreasing to 2.3×10^6 $M^{-1}s^{-1}$ at 320 mM ionic strength (Figure 5). Plotting the logarithm of the bimolecular rate constants *versus* the square root of the ionic strength according to the Brønsted law (43) yielded a Z_AZ_B parameter of −4.0, consistent with a diffusional process mediated by electrostatic interactions between the two proteins. Although the Brønsted equation is strictly applicable only to small molecules at low ionic strength, it has been widely used as an empirical measure of the importance of electrostatic interactions between redox proteins (28,50). However, it is not possible to determine whether the reaction studied here is fully or only partially diffusion-limited, and the Brønsted parameter should be considered strictly empirical. A Z_AZ_B parameter of −4.0 has also been previously found for the ET reaction between *Paracoccus* cyt c_{552} and the Cu_A-fragment of the aa_3 oxidase (24,32), suggesting that cyt c_{552} binds to both the cyt c_1 and the aa_3-oxidase through the same interaction interface.

Photoinduced electron transfer between Ru_z-23-c_{552F} and cyt c_{1CF}—The ruthenium flash photolysis method was used to study the fast ET reaction between cyt c_{1CF} and cyt c_{552F}. This method has previously been applied to characterize both intracomplex and bimolecular ET between various redox partners with microsecond time resolution (32,34,35, 39). To study the ET reaction between cyt c_{1CF} and cyt c_{552F} in the physiological direction, Ru_z-23-c_{552F} was prepared by covalently attaching the photo-excitable ruthenium compound Ru(2,2'-bipyrazine)$_2$(4-bromomethyl-4'-methyl-2,2'-bipyridine) (Ru_z) (3) to the single cysteine introduced on the surface of cyt *c*552F (N23C c_{552F}). In this position, the ruthenium complex is on the periphery of the heme crevice surface domain (Figure 1), and there should not be significant steric interference during ET complex formation. The second-order rate constant for the reaction between Ru_z-23-c_{552F} and cyt c_{1CF} was $(2.4 \pm 0.3) \times 10^7$ $M^{-1}s^{-1}$ at 8 °C and 200 mM ionic strength, compared to $(2.5 \pm 0.3) \times 10^7$ $M^{-1}s^{-1}$ for unlabeled cyt c_{552F} measured by stopped-flow spectroscopy under the same conditions. These results indicate that the ruthenium label does not affect the reaction with cyt c_{1CF} at high ionic strength. It is possible that the ruthenium complex might affect the reaction at low ionic strength, which cannot be assessed because the kinetics of wild-type cyt *c*552F cannot be measured below 50 mM ionic strength. The +2 charge on the ruthenium complex might increase the electrostatic interaction with cyt c_{1CF} at low ionic strength, favoring complex formation.

The Ru_z complex was designed to measure rapid electron transfer from cyt c_{1CF} to Ru_z-23-c_{552F} in the physicological direction (35) (Scheme 1). The driving force of the Ru_z(II*)-Fe(II) → Ru_z(I)-Fe(III) reaction (1.0 V) is close to the expected rorganization energy λ of 0.8 V for

electron transfer, allowing a maximal rate of electron transfer (35). Laser excitation of a solution containing 5.3 μM reduced cyt c_{1CF} and 4.9 μM reduced Ru_z-23-c_{552F} in 10 mM Tris/Cl, pH 8.0, resulted in rapid oxidation of heme *c* Fe(III) by photoexcited Ru_z(II*) in Ru_z-23-c_{552F} (Scheme 1), as indicated by the initial decrease in the 550 nm absorbance (Figure 3). Paraquat was present in the solution to re-oxidize Ru(I) (k_8) and prevent the thermal back reaction (k_4) in Scheme 1. The initial rapid decrease in 550 nm absorbance was followed by an exponential increase with a rate constant of 15,000 ± 3,000 s^{-1}, indicating electron transfer from cyt c_{1CF} Fe(II) to heme Fe(III) in Ru_z-23-c_{552F}. The oxidation of cyt c_{1CF} with the same rate constant was observed directly at 558 nm, an isobestic for c_{552F} (Figure 3). The observed rate constant for electron transfer between cyt c_{1CF} and Ru_z-23-c_{552F} increased linearly as the reduced cyt c_{1CF} concentration increased from 1.6 μM to 16.7 μM, indicating second-order kinetics with a second-order rate constant of $k_{12} = (3.1 \pm 0.5) \times 10^9$ $M^{-1}s^{-1}$ (Figure 4). Ascorbate and TMPD were used to keep the cytochromes reduced before flashing. At very low ionic strength it was not possible to fully reduce cyt c_{1CF} and some of its variants (as can also be deduced from the redox potentials, see Supplement 2). For this reason the reduction state of the cytochromes was checked continuously during the experiments by frequently recording absorption spectra to determine the concentration of reduced cyt c_{1CF} for calculating k_{12}. There was no indication of intracomplex electron transfer at the lowest ionic strength examined (10 mM), which would have exhibited an observed rate constant that was independent of protein concentration. The results are consistent with Scheme 2 with an equilibrium dissociation constant $K_d = k_d/k_f$ greater than 30 μM. The second-order rate constant k_{12} had a very small dependence on ionic strength from 10 mM to 35 mM, and then decreased rapidly with further increases in ionic strength (Figure 5). A Brønsted plot of log k_{12} *vs*. the square root of the ionic strength was nearly linear in the ionic strength range 40 mM to 300 mM, with a Z_AZ_B parameter of −4.85 (Figure 5). The reaction above 40 mM ionic strength can thus be described as a diffusional process mediated by long-range electrostatic interactions. The ionic strength independent phase of the bimolecular reaction below 40 mM ionic strength has not been observed before in other rapid kinetic studies of cytochromes. We propose that at ionic strengths below 40 mM, the diffusion process mediated by long-range electrostatic interactions becomes so fast that the second-order rate constant becomes rate-limited by short-range diffusion along the protein surfaces mediated by hydrophobic interactions, and is thus not affected by ionic strength. The observation of two phases in the ionic strength dependence of the reaction provides additional evidence for a two-step model of the ET reaction. A similar phenomena is observed at low ionic strength in the steady-state v_{max}/K_M parameter of some of the reactions of cyt *c* with its redox partners, including bovine and *R. sphaeroides* cyt bc_1 (17, *51*), cytochrome oxidase (50), and cytochrome *c* peroxidase (32).

Photoinduced electron transfer between yeast Ru_z-39-Cc and cyt c_{1CF}

The reaction between yeast Ru_z-39-*Cc* and cyt c_{1CF} was also studied in order to provide a comparison with the reaction between Ru_z-39-*Cc* and yeast cytochrome bc_1 which has been characterized (35) with reference to the yeast *Cc*/cyt bc_1 crystal structure (9). Laser excitation of a solution containing 5 μM Ru-39-*Cc* and 5 μM cyt c_{1CF} in 5 mM sodium phosphate, pH 7.0, led to electron transfer from the heme Fe(II) in cyt c_{1CF} to the photooxidized heme Fe(III) in Ru_z-39-*Cc* with a rate constant of 50,000 s^{-1} observed in both the 550 nm transient for heme *c* and the 557 nm transient for heme c_1 (Figure 6). The observed rate constant was independent of protein concentration above 5 μM, indicating intracomplex electron transfer between the two proteins according to Scheme 2 with $K_d = k_d/k_f < 1$ μM. The intracomplex rate constant remained nearly the same as the ionic strength was increased from 10 to 60 mM, but the amplitude of the intracomplex phase decreased as the complex dissociated, and a new slow phase appeared due to the bimolecular reaction between solution Ru_z-39-*Cc* and cyt c_{1CF}, consistent with Scheme 2 (Figure 7). The relative amplitudes of the intracomplex and bimolecular phases were 69 % and 31 % at 60 mM ionic strength, indicating an equilibrium

dissociation constant $K_d = k_d/k_f$ of 2.9 μM for the complex. The rate constant of the bimolecular phase initially increased as the ionic strength was increased from 60 to 80 mM ionic strength, indicating that the concentration of uncomplexed c_{1CF} increased over this range. At higher ionic strength the complex was fully dissociated and the rate constant decreased rapidly indicating a diffusion process mediated by long-range electrostatic interactions. The Brønsted Z_AZ_B parameter was −7.3.

The interaction between yeast Ru_z-39-*Cc* and cyt c_{1CF} was stronger than that involving Ru_z-23-c_{552F}, allowing formation of a 1:1 complex at ionic strengths below 70 mM with an intracomplex electron transfer rate constant k_{et} of 50,000 s^{-1}. The dissociation constant of the complex, K_d, was 2.9 μM at 60 mM ionic strength, and much smaller at lower ionic strength. In contrast, Ru_z-23-c_{552F} did not form a detectable complex with cyt c_{1CF} at ionic strengths down to 10 mM, and only second-order kinetics could be observed. The Brønsted parameter Z_AZ_B was larger for the reaction with Ru_z-39-*Cc* than for that with Ru_z-23-c_{552F}, indicating a stronger electrostatic interaction. In comparison, yeast Ru_z-39-*Cc* and yeast cyt bc_1 form a stable complex at low ionic strength with an intracomplex ET rate constant of 14,000 s^{-1} (35), which is independent of ionic strength between 10 and 150 mM, indicating that the complex does not change configuration within this ionic strength range. At ionic strengths above 150 mM the complex dissociates, and a bimolecular reaction is observed. The reaction between yeast Ru_z-39-*Cc* and bovine bc_1-complex has intracomplex ET kinetics at ionic strengths below 85 mM with a rate constant of 6300 s^{-1}, and becomes bimolecular at ionic strengths above 120 mM (3). The reaction between horse Ru-72-*Cc* and *Rhodobacter sphaeroides* bc_1 reveals intracomplex kinetics below 85 mM ionic strength with a rate constant of 6×10^4 s^{-1}, and becomes bimolecular at higher ionic strengths (36). Thus, the interaction between Ru_z-23-c_{552F} and cyt c_{1CF} is weaker than that of the other systems examined.

Kinetics of the ET reaction of cyt c_{1CF} mutants with Ru_z-23-c_{552F} and Ru_z-39-Cc

All cyt c_{1CF} mutants have been examined by the ruthenium photooxidation technique as described above. The effects of the mutations on the reactions with Ru_z-23-c_{552F} and yeast Ru-39-*Cc* were quite similar. The mutations can be clustered into three different regions as indicated in Figure 2. Mutations in regions II and III (A314S, K315T, G319A, S378A, Q381C, T383C) have relatively little effect on the intracomplex and second-order rate constants or the Z_AZ_B Brønsted parameter (Figure 7–Figure 10 and Table 2, Table 3). However, whereas the K315T mutant shows WT behaviour, the K315E charge inversion mutant deviates significantly from it. The charge inversion in position 315 leads to a substantial reduction of the second-order rate constants for the reactions with both Ru_z-23-c_{552F} and Ru-39-*Cc*, and shows a slight increase in the Z_AZ_B parameter compared to WT. The increased electrostatic interaction is consistent with the increased negative charge on cyt c_{1CF}, while the decreased rate constant suggests a change in the interaction interface. Mutating position S378, which corresponds to F230 in yeast involved in the cation-π-interaction, showed little effect. No other aromatic residue in close vicinity to this position could be found in the *Paracoccus* c_1 sequence.

Mutating amino acid positions in region I yielded more significant effects on the kinetics. The charge inversion mutation c_{1CF}E243K decreased the second-order rate constant for the reaction with Ru_z-23-c_{552F} to about 32 % of wild-type, but had a relatively small effect on the ionic strength dependence (Figure 9, Table 2). The intracomplex electron transfer rate constant for the reaction with Ru-39-*Cc* was decreased to 12,500 s^{-1} by the E243K mutation, while the second-order rate constant was decreased to 14 % of wild-type (Figure 7, Table 3). This charge inversion mutation appears to significantly alter the orientation of the reactive complex, thus decreasing the rate constants. The A247N mutation in region I decreased the second-order rate constants for the reactions with both Ru_z-23-c_{552F} and Ru-39-*Cc*, indicating an altered reactive complex. The region I mutants V244Q and V244T showed a rather complex effect on the

kinetics (Figure 10, Table 2, Table 3). The V244Q mutation decreased the second-order rate constants for the reactions with Ru_z-23-c_{552F} and Ru-39-*Cc* significantly, and slightly decreased the Z_AZ_B parameter for the reaction with Ru_z-23-c_{552F}. The V244T mutation significantly decreased the Z_AZ_B parameter for the reactions with both Ru_z-23-c_{552F} and Ru-39-*Cc*, and either decreased or increased the rate constant, depending on the ionic strength. Evaluation of the kinetic effects of the V244Q and V244T mutants is complicated by the fact that their redox potentials were decreased to 30 mV and 139 mV, respectively, compared with 189 mV for cyt c_{1CF} WT. Increasing the bulk and/or the polarity at residue V244 near the heme group while keeping the net charge neutral, leads to decreases in the redox potential and complex effects on the kinetics.

Taken together we propose region I as the most effective interaction interface for the ET reaction with cyt c_{552F}. Residues directly contributing to these interactions are those located directly before or within the heme binding motif (E243, V244, A274). A direct counterpart for F230 of the yeast cytochrome c_1 mediating the cation-π-interaction to cytochrome *c* (8) could not be found in the *Paracoccus* cytochrome c_1. Since the charge inverting mutations E243K and K315E led to relatively small effects on the ionic strength dependence, the bimolecular reaction between the two cytochromes appears to be mediated by long-range electrostatic interactions rather than defined ion-pairs, which is in line with the results of Tiede *et al.* (25) and the yeast cytochrome bc_1/*c* co-crystal data (7–9)..

Summary and Conclusions

The ET reaction between *Paracoccus denitrificans* cytochrome c_1 and cytochrome c_{552} was studied using soluble redox fragments of each protein. The new ruthenium derivative Ru_z-23-c_{552F} was designed to measure rapid electron transfer with cyt c_{1CF} in the physiological direction. The second-order rate constant for the ET reaction from cyt c_{1CF} to Ru_z-23-c_{552F} was nearly independent of ionic strength below 40 mM, but decreased rapidly with ionic strength above 40 mM. These results are consistent with a two-step model in which the two redox partners first approach each other in a diffusion process mediated by long-range electrostatic interactions, followed by short-range diffusion along the protein surfaces mediated by hydrophobic interactions. The empirical Brønsted parameter Z_AZ_B of −4.85 obtained from the ionic strength dependence above 40 mM is similar to that found for the reaction of cyt c_{552F} with the soluble Cu_A fragment of cytochrome *c* oxidase, strengthening the hypothesis that cyt c_{552} interacts with cyt c_1 via the same interaction interface. The interaction between yeast Ru_z-39-*Cc* and cyt c_{1CF} was stronger than that involving Ru_z-23-c_{552F}, allowing formation of a 1:1 complex at ionic strengths below 70 mM with an intracomplex electron transfer rate constant k_{et} of 50,000 s^{-1}. The complex dissociated at higher ionic strength, and the second-order rate constant decreased rapidly with increasing ionic strength with a Z_AZ_B parameter of −7.3.

To determine the interaction interface on *P. denitrificans* cyt c_1 for cyt c_{552}, a series of cyt c_{1CF} variants in the presumed docking site were prepared with reference to the yeast cyt bc_1/cyt *c* co-crystal structure (7–9). Cytochrome c_{1CF} region I (E243, V244, A247) appears to be the main interaction interface with cyt c_{552F}. Mutations having a significant effect on the kinetics involve residues located directly before or within the heme binding motif (E243, V244, A247). No direct aromatic counterpart to yeast F230 mediating the cation-π-interaction was found in *Paracoccus* cyt c_1. Mutation of cyt c_{1CF}S378, the corresponding residue indicated by the sequence alignment, showed no effect on the kinetics.

Supplementary Material

Refer to Web version on PubMed Central for supplementary material.

Acknowledgements

We thank Hans-Werner Müller for excellent technical assistance and acknowledge Maurizio Brunori ("La Sapienza" University of Rome, Italy) for making the stopped-flow apparatus available for us.

References

1. Mitchell P. Coupling of phosphorylation to electron and hydrogen transfer by a chemi-osmotic type of mechanism. Nature 1961;191:144–148. [PubMed: 13771349]
2. Gabellini N, Bowyer JR, Hurt E, Melandri BA, Hauska G. A cytochrome b/c_1 complex with ubiquinol-cytochrome c_2 oxidoreductase activity from *Rhodopseudomonas sphaeroides* GA. Eur J Biochem 1982;126(1):105–111. [PubMed: 6290210]
3. Engstrom G, Rajagukguk R, Saunders AJ, Patel CN, Rajagukguk S, Merbitz-Zahradnik T, Xiao K, Pielak GJ, Trumpower B, Yu CA, Yu L, Durham B, Millett F. Design of a ruthenium-labeled cytochrome *c* derivative to study electron transfer with the cytochrome bc_1 complex. Biochemistry 2003;42(10):2816–2824. [PubMed: 12627947]
4. Iwata S, Lee JW, Okada K, Lee JK, Iwata M, Rasmussen B, Link TA, Ramaswamy S, Jap BK. Complete structure of the 11-subunit bovine mitochondrial cytochrome bc_1 complex. Science 1998;281(5373): 64–71. [PubMed: 9651245]
5. Berry EA, Guergova-Kuras M, Huang LS, Crofts AR. Structure and function of cytochrome *bc* complexes. Annu Rev Biochem 2000;69:1005–1075. [PubMed: 10966481]
6. Hunte C, Koepke J, Lange C, Rossmanith T, Michel H. Structure at 2.3 Å resolution of the cytochrome *bc*(1) complex from the yeast *Saccharomyces cerevisiae* co-crystallized with an antibody Fv fragment. Structure 2000;8(6):669–684. [PubMed: 10873857]
7. Hunte C, Solmaz S, Lange C. Electron transfer between yeast cytochrome *bc*(1) complex and cytochrome *c*: a structural analysis. Biochim Biophys Acta 2002;1555(1–3):21–28. [PubMed: 12206886]
8. Lange C, Hunte C. Crystal structure of the yeast cytochrome bc_1 complex with its bound substrate cytochrome *c*. Proc Natl Acad Sci U S A 2002;99(5):2800–2805. [PubMed: 11880631]
9. Solmaz SR, Hunte C. Structure of complex III with bound cytochrome *c* in reduced state and definition of a minimal core interface for electron transfer. J Biol Chem 2008;283(25):17542–17549. [PubMed: 18390544]
10. Pelletier H, Kraut J. Crystal structure of a complex between electron transfer partners, cytochrome *c* peroxidase and cytochrome *c*. Science 1992;258(5089):1748–1755. [PubMed: 1334573]
11. Axelrod HL, Abresch EC, Okamura MY, Yeh AP, Rees DC, Feher G. X-ray structure determination of the cytochrome c_2: reaction center electron transfer complex from *Rhodobacter sphaeroides*. J Mol Biol 2002;319(2):501–515. [PubMed: 12051924]
12. Wienk H, Maneg O, Lücke C, Pristovsek P, Löhr F, Ludwig B, Rüterjans H. Interaction of cytochrome *c* with cytochrome *c* oxidase: an NMR study on two soluble fragments derived from *Paracoccus denitrificans*. Biochemistry 2003;42(20):6005–6012. [PubMed: 12755602]
13. Muresanu L, Pristovsek P, Löhr F, Maneg O, Mukrasch MD, Rüterjans H, Ludwig B, Lücke C. The electron transfer complex between cytochrome c_{552} and the Cu_A domain of the *Thermus thermophilus* ba_3 oxidase. A combined NMR and computational approach. J Biol Chem 2006;281 (20):14503–14513. [PubMed: 16554303]
14. Sarewicz M, Borek A, Daldal F, Froncisz W, Osyczka A. Demonstration of short-lived complexes of cytochrome *c* with cytochrome bc_1 by EPR spectroscopy: Implications for the mechanism of interprotein electron transfer. J Biol Chem. 2008in press
15. Speck SH, Ferguson-Miller S, Osheroff N, Margoliash E. Definition of cytochrome *c* binding domains by chemical modification: kinetics of reaction with beef mitochondrial reductase and functional organization of the respiratory chain. Proc Natl Acad Sci U S A 1979;76(1):155–159. [PubMed: 218193]
16. Rieder R, Bosshard HR. Comparison of the binding sites on cytochrome *c* for cytochrome *c* oxidase, cytochrome bc_1, and cytochrome c_1. Differential acetylation of lysyl residues in free and complexed cytochrome c. J Biol Chem 1980;255(10):4732–4739. [PubMed: 6246081]

17. Hall J, Zha XH, Yu L, Yu CA, Millett F. The binding domain on horse cytochrome *c* and *Rhodobacter sphaeroides* cytochrome c_2 for the *Rhodobacter sphaeroides* cytochrome bc_1 complex. Biochemistry 1987;26(14):4501–4504. [PubMed: 2822095]
18. Hall J, Zha XH, Yu L, Yu CA, Millett F. Role of specific lysine residues in the reaction of *Rhodobacter sphaeroides* cytochrome c_2 with the cytochrome bc_1 complex. Biochemistry 1989;28(6):2568–2571. [PubMed: 2543445]
19. Nakai M, Endo T, Hase T, Tanaka Y, Trumpower BL, Ishiwatari H, Asada A, Bogaki M, Matsubara H. Acidic regions of cytochrome c_1 are essential for ubiquinol-cytochrome *c* reductase activity in yeast cells lacking the acidic QCR6 protein. J Biochem (Tokyo) 1993;114(6):919–925. [PubMed: 8138552]
20. Ubbink M, Ejdeback M, Karlsson BG, Bendall DS. The structure of the complex of plastocyanin and cytochrome *f*, determined by paramagnetic NMR and restrained rigid-body molecular dynamics. Structure 1998;6(3):323–335. [PubMed: 9551554]
21. Witt H, Malatesta F, Nicoletti F, Brunori M, Ludwig B. Cytochrome-*c*-binding site on cytochrome oxidase in *Paracoccus denitrificans*. Eur J Biochem 1998;251(1–2):367–373. [PubMed: 9492306]
22. Drosou V, Malatesta F, Ludwig B. Mutations in the docking site for cytochrome *c* on the *Paracoccus* heme aa_3 oxidase. Electron entry and kinetic phases of the reaction. Eur J Biochem 2002;269(12):2980–2988. [PubMed: 12071962]
23. Drosou V, Reincke B, Schneider M, Ludwig B. Specificity of the interaction between the *Paracoccus denitrificans* oxidase and its substrate cytochrome *c*: comparing the mitochondrial to the homologous bacterial cytochrome *c*(552), and its truncated and site-directed mutants. Biochemistry 2002;41(34): 10629–10634. [PubMed: 12186548]
24. Maneg O, Ludwig B, Malatesta F. Different interaction modes of two cytochrome-*c* oxidase soluble Cu_A fragments with their substrates. J Biol Chem 2003;278(47):46734–46740. [PubMed: 12937163]
25. Tiede DM, Vashishta AC, Gunner MR. Electron-transfer kinetics and electrostatic properties of the *Rhodobacter sphaeroides* reaction center and soluble *c*- cytochromes. Biochemistry 1993;32(17): 4515–4531. [PubMed: 8387335]
26. Kurowski B, Ludwig B. The genes of the *Paracoccus denitrificans* bc_1 complex. Nucleotide sequence and homologies between bacterial and mitochondrial subunits. J Biol Chem 1987;262(28):13805–13811. [PubMed: 2820981]
27. Janzon J, Eichhorn AC, Ludwig B, Malatesta F. Electron transfer kinetics between soluble modules of *Paracoccus denitrificans* cytochrome c_1 and its physiological redox partners. Biochim Biophys Acta 2008;1777(3):250–259. [PubMed: 18241666]
28. Stonehuerner J, O'Brien P, Geren L, Millett F, Steidl J, Yu L, Yu CA. Identification of the binding site on cytochrome c_1 for cytochrome *c*. J Biol Chem 1985;260(9):5392–5398. [PubMed: 2985591]
29. Turba A, Jetzek M, Ludwig B. Purification of *Paracoccus denitrificans* cytochrome c_{552} and sequence analysis of the gene. Eur J Biochem 1995;231(1):259–265. [PubMed: 7628479]
30. Harrenga A, Reincke B, Rüterjans H, Ludwig B, Michel H. Structure of the soluble domain of cytochrome *c*(552) from *Paracoccus denitrificans* in the oxidized and reduced states. J Mol Biol 2000;295(3):667–678. [PubMed: 10623555]
31. Witt H, Malatesta F, Nicoletti F, Brunori M, Ludwig B. Tryptophan 121 of subunit II is the electron entry site to cytochrome-*c* oxidase in *Paracoccus denitrificans*. Involvement of a hydrophobic patch in the docking reaction. J Biol Chem 1998;273(9):5132–5136. [PubMed: 9478966]
32. Maneg O, Malatesta F, Ludwig B, Drosou V. Interaction of cytochrome *c* with cytochrome oxidase: two different docking scenarios. Biochim Biophys Acta 2004;1655(1–3):274–281. [PubMed: 15100042]
33. Mooser D, Maneg O, Corvey C, Steiner T, Malatesta F, Karas M, Soulimane T, Ludwig B. A four-subunit cytochrome *bc*(1) complex complements the respiratory chain of *Thermus thermophilus*. Biochim Biophys Acta 2005;1708(2):262–274. [PubMed: 15869739]
34. Wang K, Mei H, Geren L, Miller MA, Saunders A, Wang X, Waldner JL, Pielak GJ, Durham B, Millett F. Design of a ruthenium-cytochrome *c* derivative to measure electron transfer to the radical cation and oxyferryl heme in cytochrome *c* peroxidase. Biochemistry 1996;35(47):15107–15119. [PubMed: 8942678]

35. Sadoski RC, Engstrom G, Tian H, Zhang L, Yu CA, Yu L, Durham B, Millett F. Use of a photoactivated ruthenium dimer complex to measure electron transfer between the Rieske iron-sulfur protein and cytochrome *c*(1) in the cytochrome *bc*(1) complex. Biochemistry 2000;39(15):4231–4236. [PubMed: 10757970]
36. Tian H, Sadoski R, Zhang L, Yu CA, Yu L, Durham B, Millett F. Definition of the interaction domain for cytochrome c on the cytochrome *bc*(1) complex. Steady-state and rapid kinetic analysis of electron transfer between cytochrome *c* and *Rhodobacter sphaeroides* cytochrome *bc*(1) surface mutants. J Biol Chem 2000;275(13):9587–9595. [PubMed: 10734109]
37. Arslan E, Schulz H, Zufferey R, Kunzler P, Thöny-Meyer L. Overproduction of the *Bradyrhizobium japonicum c*- type cytochrome subunits of the cbb_3 oxidase in *Escherichia coli*. Biochem Biophys Res Commun 1998;251(3):744–747. [PubMed: 9790980]
38. Witholt B, Boekhout M, Brock M, Kingma J, Heerikhuizen HV, Leij LD. An efficient and reproducible procedure for the formation of spheroplasts from variously grown *Escherichia coli*. Anal Biochem 1976;74(1):160–170. [PubMed: 786067]
39. Schägger H, von Jagow G. Tricine-sodium dodecyl sulfate-polyacrylamide gel electrophoresis for the separation of proteins in the range from 1 to 100 kDa. Anal Biochem 1987;166(2):368–379. [PubMed: 2449095]
40. Thomas PE, Ryan D, Levin W. An improved staining procedure for the detection of the peroxidase activity of cytochrome P-450 on sodium dodecyl sulfate polyacrylamide gels. Anal Biochem 1976;75(1):168–176. [PubMed: 822747]
41. Pristovsek P, Lücke C, Reincke B, Ludwig B, Rüterjans H. Solution structure of the functional domain of *Paracoccus denitrificans* cytochrome c_{552} in the reduced state. Eur J Biochem 2000;267(13):4205–4212. [PubMed: 10866825]
42. Berry EA, Trumpower BL. Simultaneous determination of hemes *a*, *b*, and *c* from pyridine hemochrome spectra. Anal Biochem 1987;161(1):1–15. [PubMed: 3578775]
43. Brønsted JN, La Mer VK. The activity coefficients of ions in very dilute solutions. J. Am. Chem. Soc 1924;46(3):555–573.
44. Heacock DH 2nd, Liu RQ, Yu CA, Yu L, Durham B, Millett F. Intracomplex electron transfer between ruthenium-cytochrome *c* derivatives and cytochrome c_1. J Biol Chem 1993;268(36):27171–27175. [PubMed: 8262956]
45. Schoppink PJ, Hemrika W, Berden JA. The effect of deletion of the genes encoding the 40 kDa subunit II or the 17 kDa subunit VI on the steady-state kinetics of yeast ubiquinol-cytochrome-*c* oxidoreductase. Biochim Biophys Acta 1989;974(2):192–201. [PubMed: 2540835]
46. Thompson JD, Higgins DG, Gibson TJ. CLUSTAL W: improving the sensitivity of progressive multiple sequence alignment through sequence weighting, position-specific gap penalties and weight matrix choice. Nucleic Acids Res 1994;22(22):4673–4680. [PubMed: 7984417]
47. Peitsch MC, Wells TN, Stampf DR, Sussman JL. The Swiss-3DImage collection and PDB-Browser on the World-Wide Web. Trends Biochem Sci 1995;20(2):82–84. [PubMed: 7701568]
48. Bates PA, Kelley LA, MacCallum RM, Sternberg MJ. Enhancement of protein modeling by human intervention in applying the automatic programs 3D-JIGSAW and 3D-PSSM. Proteins 2001:39–46. [PubMed: 11835480]
49. Lambert C, Leonard N, De Bolle X, Depiereux E. ESyPred3D: Prediction of proteins 3D structures. Bioinformatics 2002;18(9):1250–1256. [PubMed: 12217917]
50. Smith HT, Ahmed AJ, Millett F. Electrostatic interaction of cytochrome *c* with cytochrome c_1 and cytochrome oxidase. J Biol Chem 1981;256(10):4984–4990. [PubMed: 6262312]

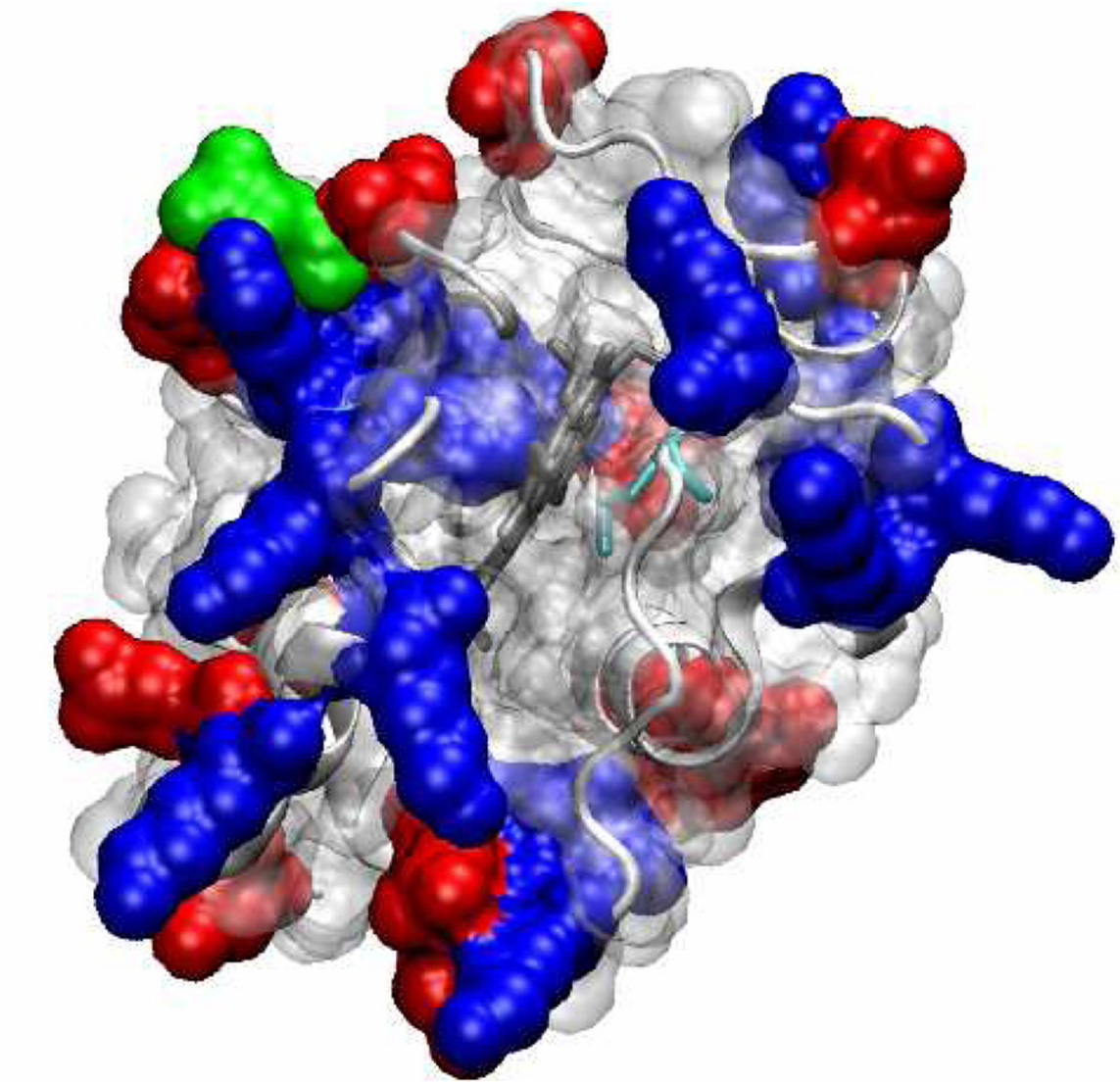

Figure 1.
Surface representation of *Paracoccus denitrificans* cytochrome c_{552F} (1QL4, [30]) viewed toward the heme crevice and potential interaction interface with cytochrome c_{1CF}. The overall surface (white) is partially transparent, allowing visualization of the heme group (grey), the distal heme ligand met 78 (cyan) and the cytochrome backbone fold (light grey). Basic residues (blue) surround the heme cleft, whereas the acidic residues (red) are located at its periphery or on the c_{552F} reverse side. Asparagine 23, which was mutated to cysteine and covalently attached to the ruthenium complex in Ru_z-23-c_{552F}, is marked in green.

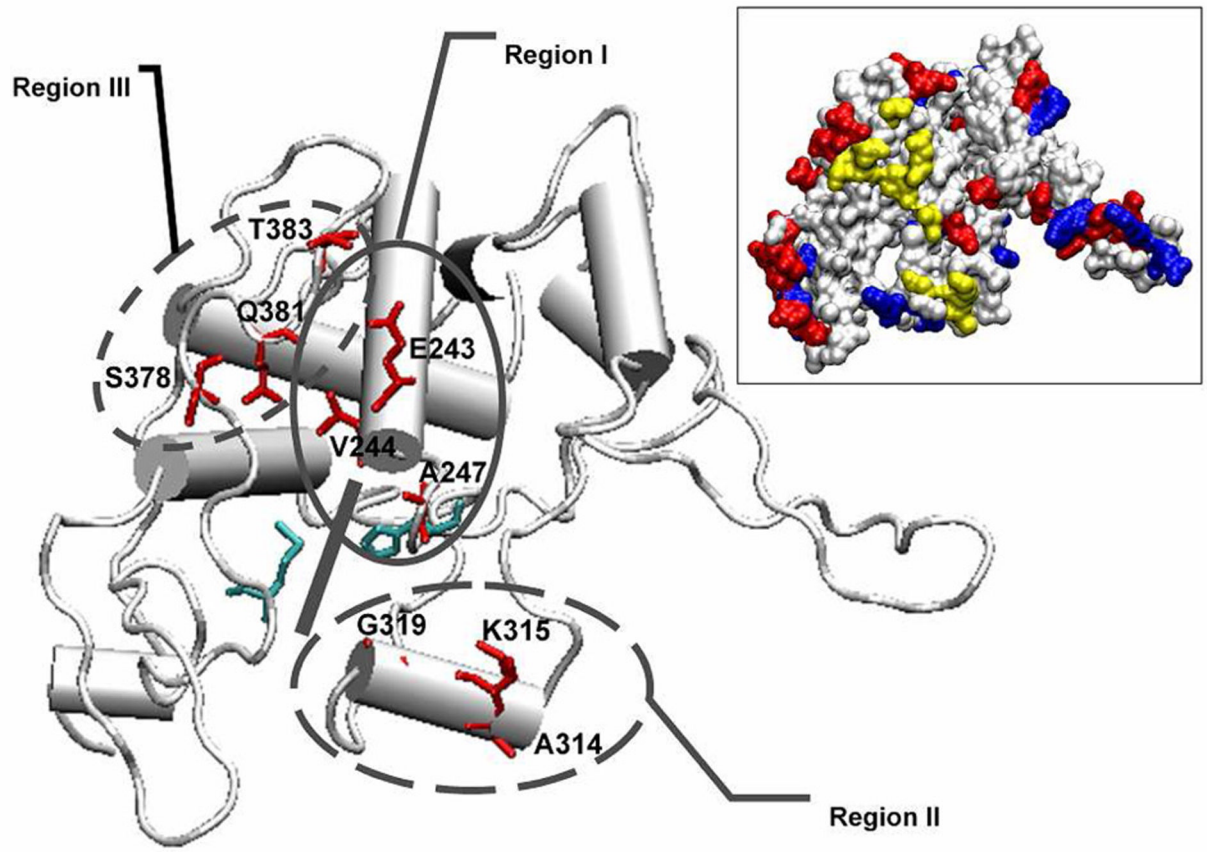

Figure 2.

Paracoccus denitrificans cytochrome c_{1CF} sequence modelled onto the yeast *Saccharomyces cerevisiae* cytochrome c_1 structure (1KYO pdb, [8]) using Swissmodell [47]. The view is towards the heme crevice and membrane plane along the transmembrane helix (TMH). Regions I-III as designated (for further details see text), red: positions for mutagenesis; cyan: axial and distal heme ligands (M373 and H249); dark grey bar: simulated heme group. Inset: Cyt c_{1CF} surface representation (same orientation as in Figure 2). Mutated positions are shown in yellow, basic residues in blue. Acidic residues (red) form a distant ring around the heme cleft.

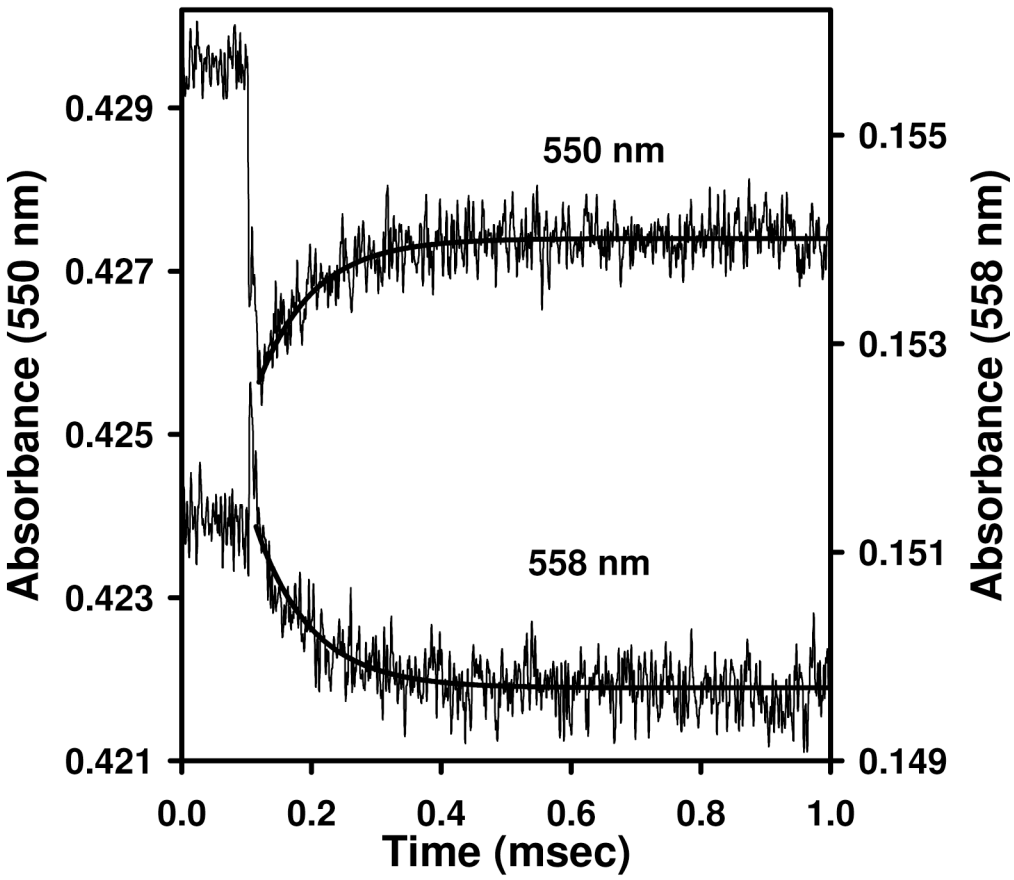

Figure 3.

Photoinduced electron transfer between cyt c_{1CF} wild-type and Ru_z-23-c_{552F}. A solution containing 5.3 μM cyt c_{1CF} and 4.9 μM Ru_z-23-c_{552F} in 10 mM Tris/Cl buffer (pH 8.0), 100 μM ascorbate, 1 mM paraquat and 2 μM TMPD at 25 °C was excited with a 480 nm laser flash of 0.5 μs duration. Cytochromec_{552F} oxidation and rereduction by cytochrome c_{1CF} were monitored at 550 nm, and cytochrome c_{1CF} oxidation was monitored at 558 nm. The sharp upward spike in the 558 nm transient is due to a light-scattering artifact. The rate constant for the exponential transients at both wavelengths is 15,000 s^{-1}.

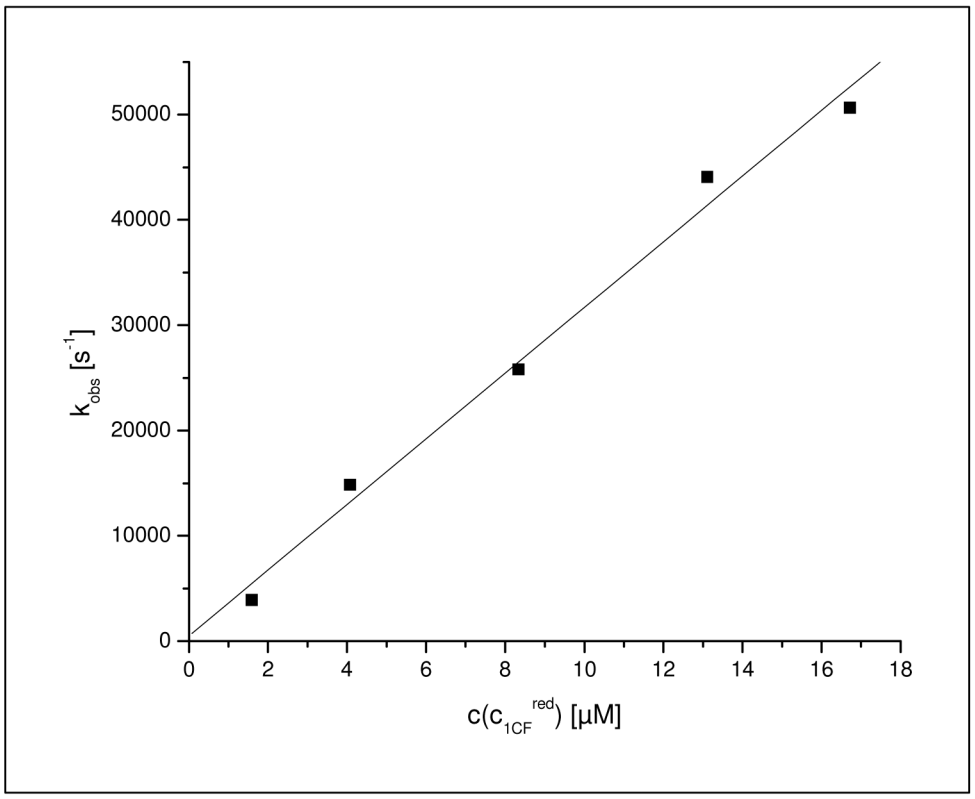

Figure 4.

Concentration dependence of photoinduced electron transfer between cyt c_{1CF} wild-type and Ru_z-23-c_{552F}. The conditions were the same as in Figure 3 except that the cyt c_{1CF} concentration was varied from 1.6 μM to 16.7 μM. The slope of the plot yielded a second-order rate constant k_{12} of 3.1×10^9 $M^{-1}s^{-1}$.

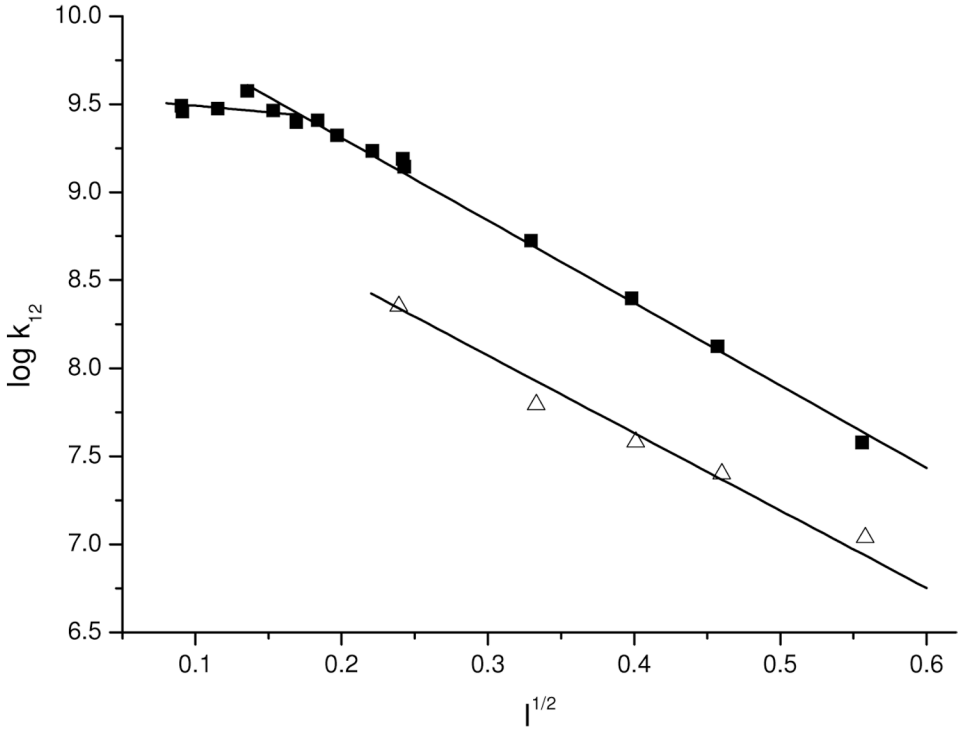

Figure 5.

Ionic strength dependence of second-order rate constants for the photoinduced electron transfer between wild-type cyt c_{1CF} and Ru_z-23-c_{552F} (■), and for electron transfer between cyt c_{1CF} and wild-type cyt c_{552F} measured by stopped-flow spectroscopy (△). The conditions for photoinduced electron transfer were the same as in Figure 3, with KCl added to increase the ionic strength. The stopped-flow spectroscopy experiments involving wild-type cyt c_{552F} were carried out at 8 °C.

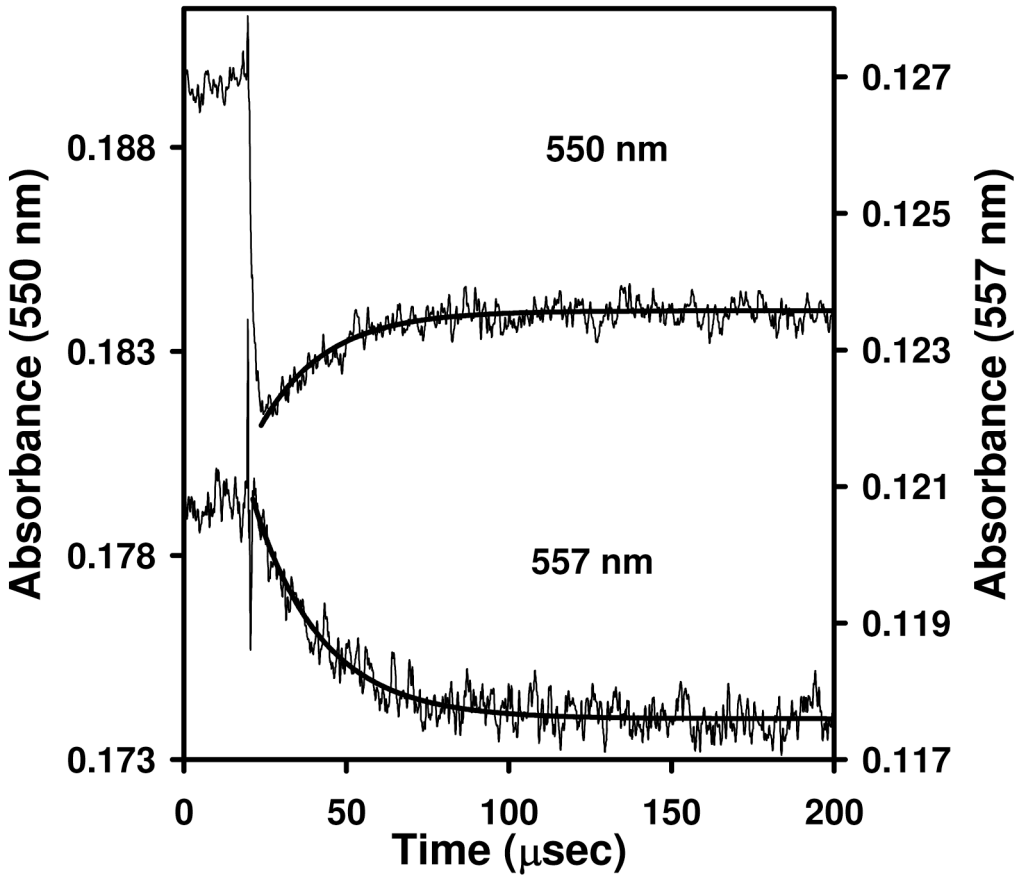

Figure 6.

Photoinduced electron transfer between cyt c_{1CF} wild-type and yeast Ru-39-*Cc*. A solution containing 5 μM cyt c_{1CF} and 5 μM Ru_z-39-*Cc* in 5 mM sodium phosphate, pH 7.0, 100 μM ascorbate, and 2 μM TMPD was excited with a 480 nm laser flash of 0.5 μs duration. Ru-39-*Cc* photooxidation and rereduction were monitored at 550 nm, and cytochrome c_{1CF} oxidation was monitored at 557 nm.

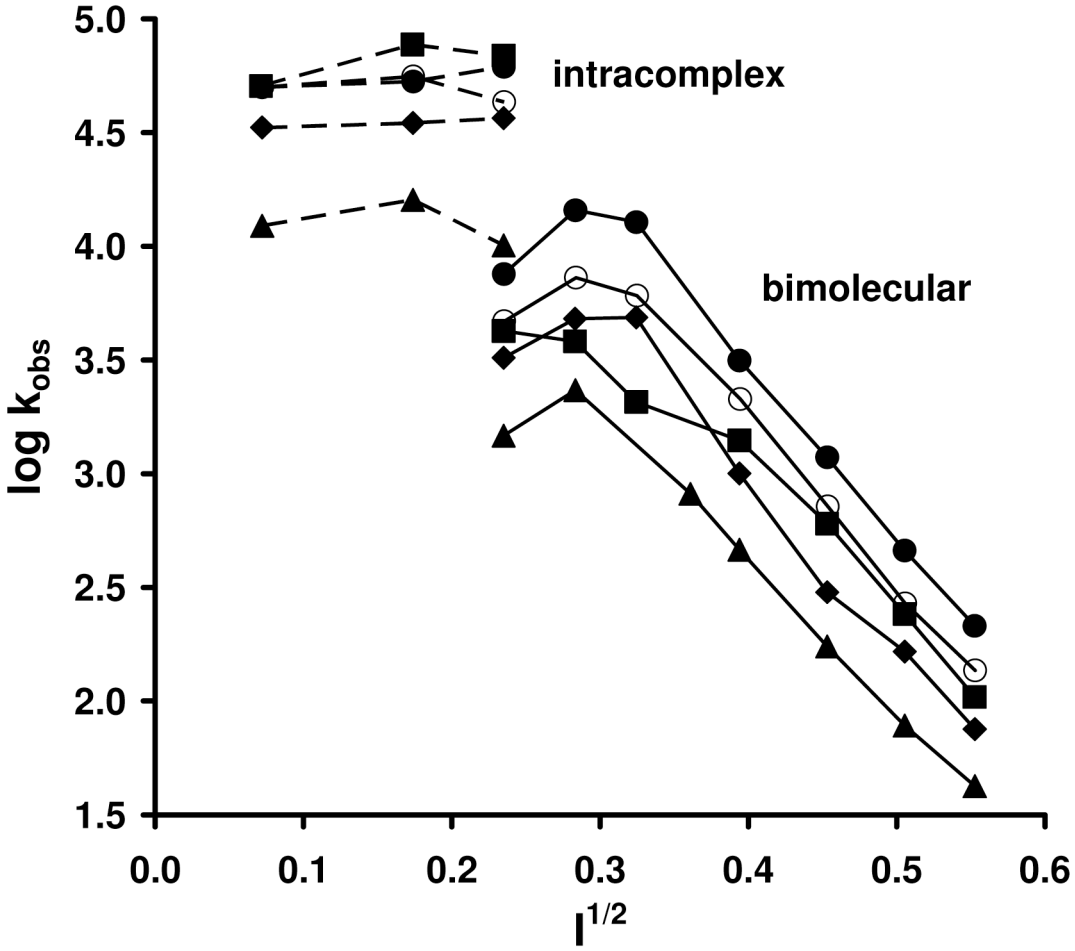

Figure 7.

Ionic strength dependence of photoinduced electron transfer between Ru_z-39-*Cc* and cyt c_{1CF} wild-type and mutants. Solutions contained 10 μM cyt c_{1CF} and 5 μM Ru_z-39-*Cc* in 5 mM sodium phosphate, pH 7.0, 100 μM ascorbate, 2 μM TMPD and 0– 300 mM NaCl at 25 °C: c_{1CF} wild-type (●), S378A (○), K315E (◆), A247N (■) and E243K (▲). The upper curves at low ionic strength are intracomplex rate constants, while the lower curves at higher ionic strengths are k_{obs} values for the bimolecular reactions.

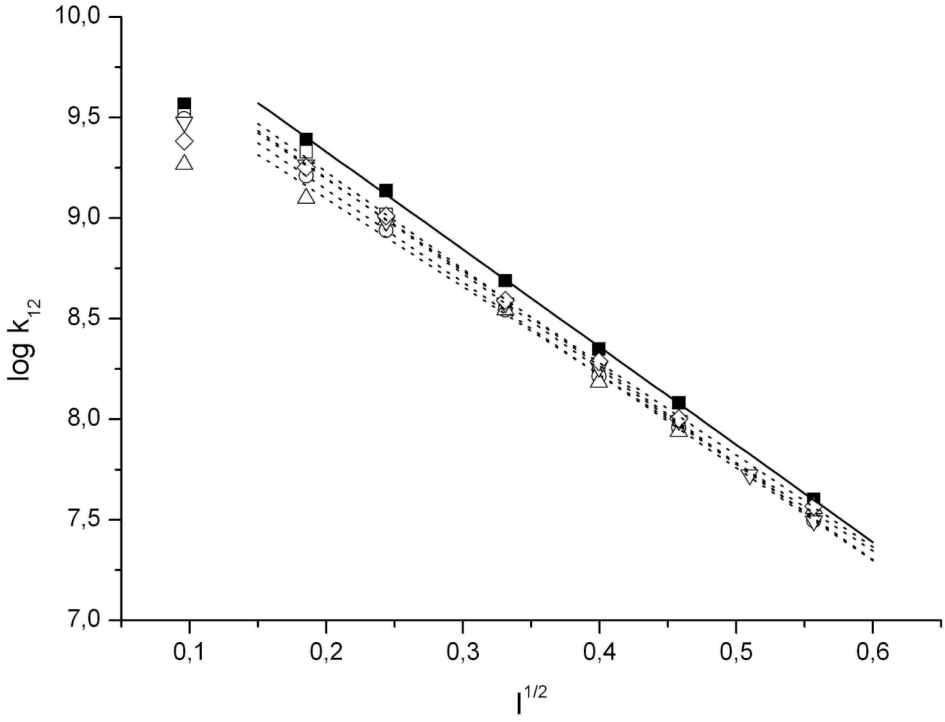

Figure 8.

Ionic strength dependency of the second-order rate constants k_{12} of the ET reaction between cytochrome c_{1CF} wild-type and Ru_z-23-c_{552F} compared to cyt c_{1CF} mutants with similar k_{12} values and ionic strength behaviour measured by flash photolysis experiments (T = 25 °C): c_{1CF} wild-type (■), K315T (□), G319A (○), A314S (△), S378A (▽) and Q381V (◇); full line: fitted Brønsted plot for the bimolecular ET reaction of cytochrome c_{1CF} wild-type, dotted lines: fitted Brønsted plot for the bimolecular ET reaction of cytochrome c_{1CF} mutants.

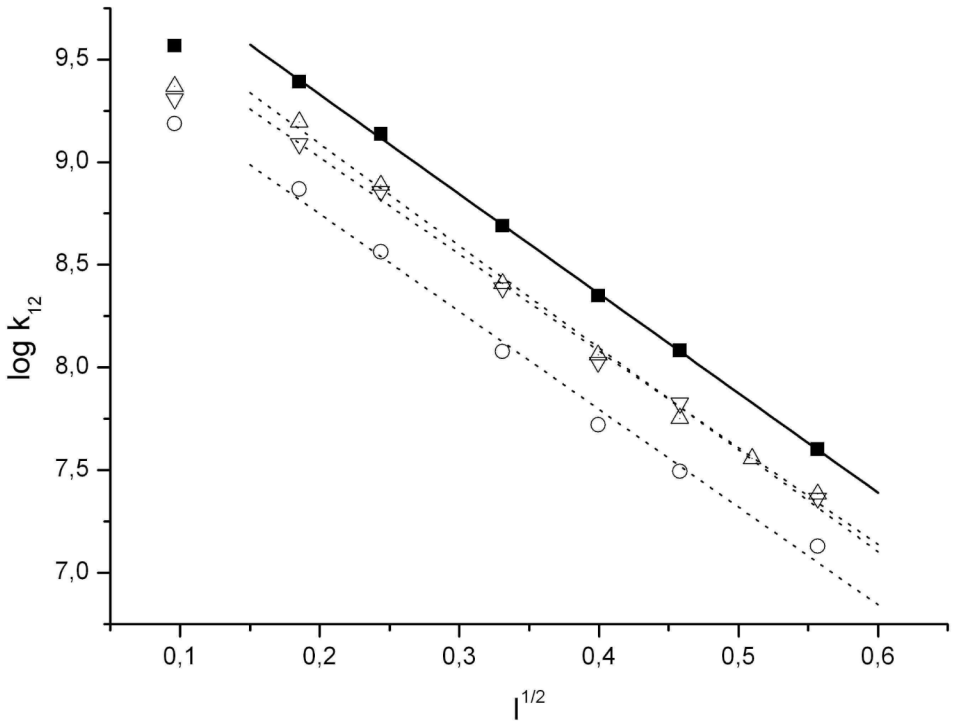

Figure 9.

Ionic strength dependency of the second-order rate constants k_{12} of the ET reaction between cytochrome c_{1CF} wild-type and Ru_z-23-c_{552F} compared to mutants with changed k_{12} values but similar ionic strength behaviour measured by flash photolysis experiments (T = 25 °C): c_{1CF} wild-type (■), E243K (△), A247N (○) and T383C (▽); full line: fitted Brønsted plot for the bimolecular ET reaction of cytochrome c_{1CF} wild-type, dotted lines: fitted Brønsted plot for the bimolecular ET reaction of cytochrome c_{1CF} mutants.

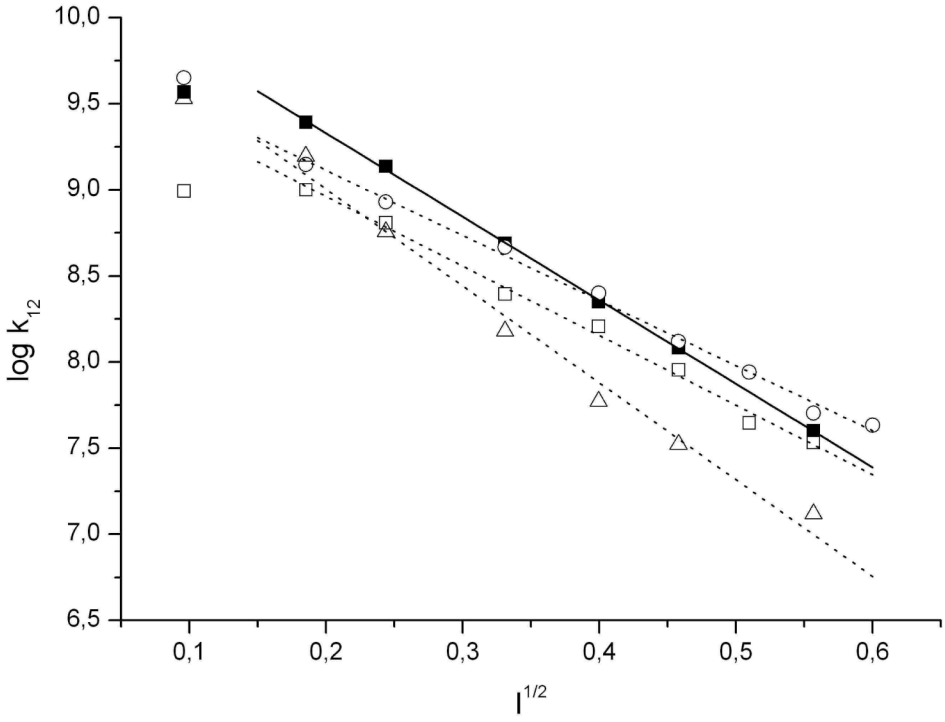

Figure 10.

Ionic strength dependency of the second-order rate constants k_{12} of the ET reaction between cytochrome c_{1CF} wild-type and Ru_z-23-c_{552F} compared to mutants with changed k_{12} and ionic strength behaviour measured by flash photolysis experiments (T = 25 °C): c_{1CF} wild-type (■), V244Q (□), V244T (○) and K315E (△); full line: fitted Brønsted plot for the bimolecular ET reaction of cytochrome c_{1CF} wild-type, dotted lines: fitted Brønsted plot for the bimolecular ET reaction of cytochrome c_{1CF} mutants

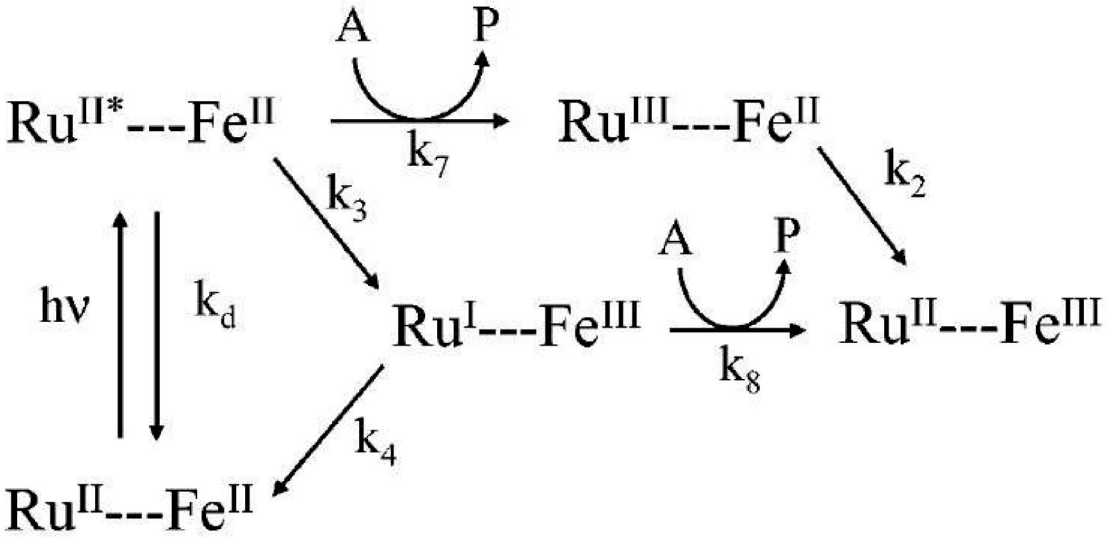

Scheme 1.

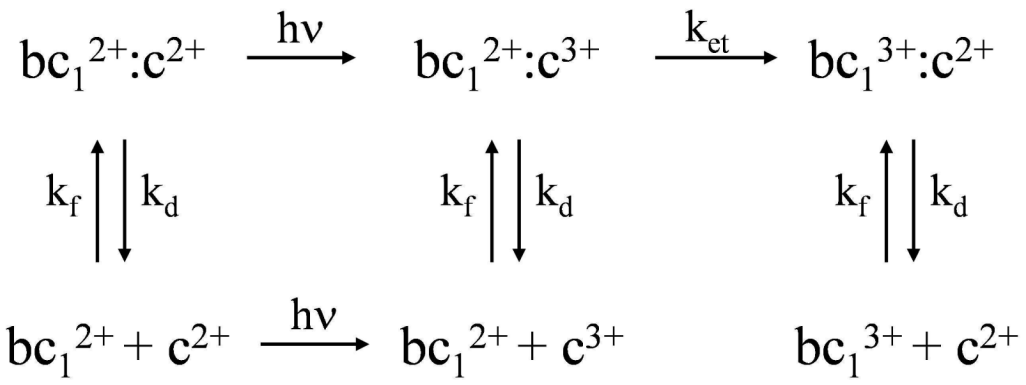

Scheme 2.

Table 1

Amino acid positions on cytochrome c_1 of the yeast bc_1/ cyt *c* co-complex crystal (1KYO, pdb (8)) mediating direct interactions to cytochrome *c*, corresponding residues on *P. denitrificans* cytochrome c_1 and site-directed mutations.

Amino acid position in yeast cyt$_1$	Amino acid position in *P. denitrificans* cyt c_1	Mutations
E99[a]	E243	E243K
V100[a]	V244	V244Q, T
A103	A247	A247N
A164	A314	A314S
	K315	K315E,T
A168	G319	G319A
F230	S378	S378A
M233	Q381	Q381V
E235	T383	T383C

[a]E99 and V100 do not show direct interactions in the yeast co-complex, but are surface exposed in the *S. c.* structure and were additionally chosen for mutagenesis

Table 2

Effect of cyt c_{1CF} mutants on the kinetics of photoinduced ET with Ru_z-23-c_{552F}. The conditions are the same as in Figure 5. The percent wild-type activity is the percent of the second-order rate constant of the mutant relative to wild-type at ionic strengths ranging from 35 mM to 300 mM. The Brønsted parameter Z_AZ_B was determined over this same ionic strength range and its negative sign implies attractive forces between two oppositely charged partners.

Cyt c_{1CF}	Region	% of WT activity[b]	Z_AZ_B
wt	-	100	−4.85
E243K	I	31–34	−4.95
V244Q	I	47–85	−4.03
V244T	I	62–126	−3.78
A247N	I	60–66	−4.97
A314S	II	75–78	−4.61
K315E	II	17–49	−5.54
K315T	II	86–90	−4.82
G319A	II	84–90	−4.60
S378A	III	78–83	−4.74
Q381V	III	88–93	−4.57
T383C	III	57–62	−4.71

[b] depending on ionic strength conditions

Table 3

Effect of cyt c_{1CF} mutants on the kinetics of photoinduced ET with yeast Ru-39-*Cc*. The conditions were the same as in Figure 7. The intracomplex electron transfer rate constant k_{et} was measured at 10 mM ionic strength. The second-order rate constant k_{12} was measured at 160 mM ionic strength. The Brønsted parameter Z_AZ_B was measured between 100 mM and 300 mM ionic strength.

Cyt c_{1CF}	Region	k_{et} (s^{-1})	k_{12} (10^8 $M^{-1}s^{-1}$)	$-Z_AZ_B$
wt	–	50,000	3.5 (100%)	7.3
E243K	I	12,500	0.50 (14%)	6.5
V244Q	I	55,000	2.2 (63%)	7.3
V244T	I	44,000	3.7 (106%)	5.2
A247N	I	55,000	1.6 (46%)	6.7
A314S	II	46,000	2.3 (66%)	7.1
K315E	II	34,000	1.1 (31%)	7.8
K315T	II	38,000	3.5 (100%)	7.3
G319A	II	44,000	3.0 (86%)	6.5
S378A	III	50,000	2.2 (63%)	6.3
Q381V	III	60,000	4.1 (117%)	6.6